# Characterisation of solidification using combined Confocal Scanning Laser Microscopy with Infrared Thermography.

Carl Slater[1], Kateryna Hechu[1] and Seetharaman Sridhar[1]

[1]University of Warwick

c.d.slater@warwick.ac.uk

## Abstract

Confocal scanning laser microscopy is a growing technique as it offers the unique capability to observe (amongst other things) the solidification of high melting point materials such as steels. Here this technique has been expanded to incorporate an infrared thermographer to gain bulk information about solidification of both pure iron and a low carbon steel. This technique shows a clear indication of the onset and competition of solidification at rates up to 10 °C/s and as such becomes more applicable to the rates expected during steel casting compared to conventional calorimetry.

## Highlights

- An upgrade of the CSLM has been proposed that incorporates thermography.
- Solidification has been successfully monitored using this technique
- Comparisons has been made to conventional DSC techniques.

# Characterisation of solidification using combined Confocal Scanning Laser Microscopy with Infrared Thermography.

## 1. ABSTRACT

Confocal scanning laser microscopy is a growing technique as it offers the unique capability to observe (amongst other things) the solidification of high melting point materials such as steels. Here this technique has been expanded to incorporate an infrared thermographer to gain bulk information about solidification of both pure iron and a low carbon steel. This technique shows a clear indication of the onset and competition of solidification at rates up to 10 °C/s and as such becomes more applicable to the rates expected during steel casting compared to conventional calorimetry.

Keywords: Solidification, thermography, in-situ, casting

## 2. INTRODUCTION

With the ever increasing drive to lower emissions and increase efficiency then fabrication of metallic alloys has moved to more novel methods. This can be seen in industries such as aluminium sheet fabrication where companies such as Alcoa have used modern belt casting techniques to reduce production times from days to minutes [1]. This is also seen in the steel industry where belt casting and twin rolling technologies are emerging [2,3]. With these new technologies comes new scientific challenges. One of the specific challenges related to these technologies is that due to the accelerated manufacturing of these products, an acceleration in the solidification rate is seen, and this can have a significant impact on the resultant microstructure.

With regards to steelmaking, conventional continuous casting has been in implementation since the 1970's [2] and although offering the capability to make semi-finished product continuously, solidification rates remained slow and comparable to its ingot casting counterpart (bulk solidification rates of < 1 C/s [4]). For this, conventional techniques for analysing solidification such as Differential Scanning Calorimetry (DSC) were sufficient. However, these newer steelmaking techniques involve much faster cooling rates (belt casting for example shows up to 50 °C/s), and are beyond the capability of DSC (typically around 0.1-0.5 °C/s).

Confocal Scanning Laser Microscope has been shown to offer a greater control over thermal profiles compared to other analytic machines (heating and cooling rates of >50 °C/s can be achieved [5], in addition to this the CSLM is capable of imaging the specimen and offer good environmental control over the DSC. Although optically many physical transformations can be seen in the CSLM, there is merit in being able to define transformations through latent heat of transformation, as optically it relies heavily on the quality of the surface (which is dictated by the atmosphere, type of phase(s) formed during solidification, inclusions present). Visual imaging through CSLM relies on the appearances of surface relief structures on the surface causing topological variances. When these are subtle due to slow transformation rates or rapid surface diffusion smoothing out features on the surface it becomes hard to quantify the evolution. The objective of this work is to establish if thermal imaging in conjuncture with visual observation can be used to enhance the capabilities of the CSLM.

## 3. EXPERIMENTAL

### 3.1. Adaption of the CSLM to image using Infrared Thermography

Use of high temperature CSLM, pioneered by Emi and co-workers at Tohoku University [6–8], and the mechanism of how it works has been documented and explained in detail in literature [5,9–15]. Figure 1 shows a schematic of the set up used in this report. The CSLM used in this work is a Yonekura VL2000DX-SVF17SP. In a conventional CSLM setup a He-Ne laser is used as an imagining source, however the method proposed here allows the laser to be quickly switched for Infrared Thermographer (IRT).

IRTs typically operate at one of two frequency ranges, either around 1-1.5 µm or 8-14 µm. The halogen bulb used as a heat source in this set up operates at a frequency 300-2000 nm, therefore any imaging source that is used needs to operate at frequencies higher than 2 µm.

The viewing window is conventionally fabricated from quartz due to its thermal stability and high transmissivity around the laser operating frequency. However, quartz transmissivity drops significantly after 4 µm. Therefore, for this experimental procedure a $CaF_2$ window was used which maintains >70% transmissivity up to 14 µm which allowed the usage of a Micro Epsilon TIM 160 thermal imaging camera operating at a frequency of 7.6-13 µm, recording at 120 Hz with a resolution of 160x120 pixels using a 6° lens. This camera has a thermal sensitivity of 0.04K.

The thermographer is clamped 45 mm above the viewing window (allowing air flow around the lens prevents overheating and warping). The camera is then manually focused to the surface of the sample. Radiated heat was calculated by the following equation:

$$\frac{Q}{A} = \varepsilon \sigma T^4$$

Where Q is the heat transfer per unit time, σ is the Stefan-Boltzmann constant, T is the absolute temperature and ε is the emissivity of the sample. A value for ε of 0.3 was used for this study which is consistent with liquid steel, this provides an effective temperature which is then used in this equation. The thermographer receives an IR signal from the sample which corresponds to specific energy values, the software then automatically converts this to a temperature for a given emissivity. Therefore, back calculating this means that the accuracy of emissivity is less important, it is only the apparent temperature at a specified emissivity that is needed. This reduces the noise significantly. The spot size used in this study was 0.059 $mm^2$.

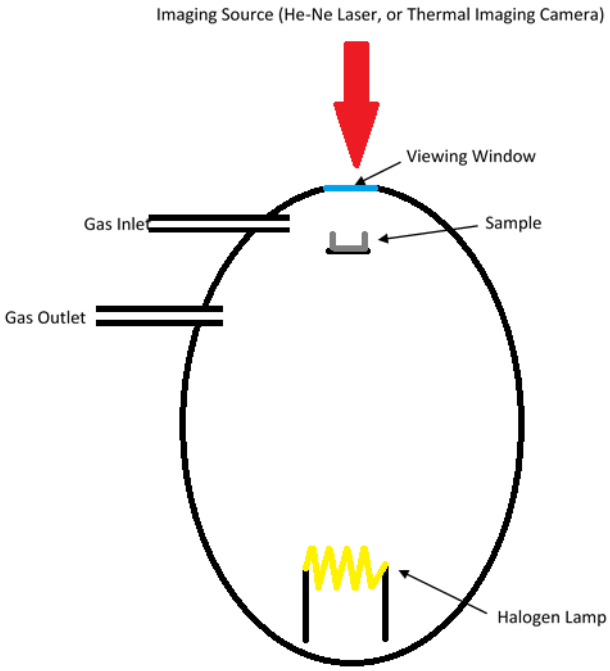


**Figure 1: Schematic diagram showing the experimental set up of the confocal scanning laser microscope.**

### 3.2. Solidification Trials

Prior to testing the CSLM is calibrated using four pure metals (Al, Au, Ni and Fe) of the same geometry, and heated to 100 °C below the expected melting point at 10 °C/s. The sample is then heated at 0.5 C/s, and the melting points are verified. This process is repeated three times for each element.

For these trials an electrolytically pure iron (99.999% Fe) and a low carbon steel (0.042C, 0.234Mn) were chosen. Samples of each material were sectioned down to 3 mm cubes and placed in an alumina crucible. The CSLM chamber was then evacuated and backfilled with N6 argon three times before starting each test using a flow rate of 300 mL/min.

Samples were initially heated to 200 °C for 2mins to dry the sample and chamber before heating to 1350 °C at a rate of 4 °C/s, and then to 1600 °C at a rate of 1 °C/s. The sample was held for 30 seconds before cooling to 1200 °C at 1 °C/s, and they let naturally cool to room temperature. This was repeated with a 10 °C/s cooling rate from 1600 °C to 1200 °C. All tests were repeated at least one for each sample and condition.

## 4. RESULTS AND DISCUSSION

As a benchmark Figure 2 shows the DSC cooling curves for both the pure iron and the low carbon steel. This was measured at 0.5 °C/s in a NETZSCH STA 449 F3 *Jupiter* DSC which is the top end of the achievable cooling rates in this model. It can be seen that the liquidus temperature for the pure iron and low carbon steel is 1520 and 1495 °C respectively. The onset of delta ferrite to austenite transformation occurs at 1425 °C.

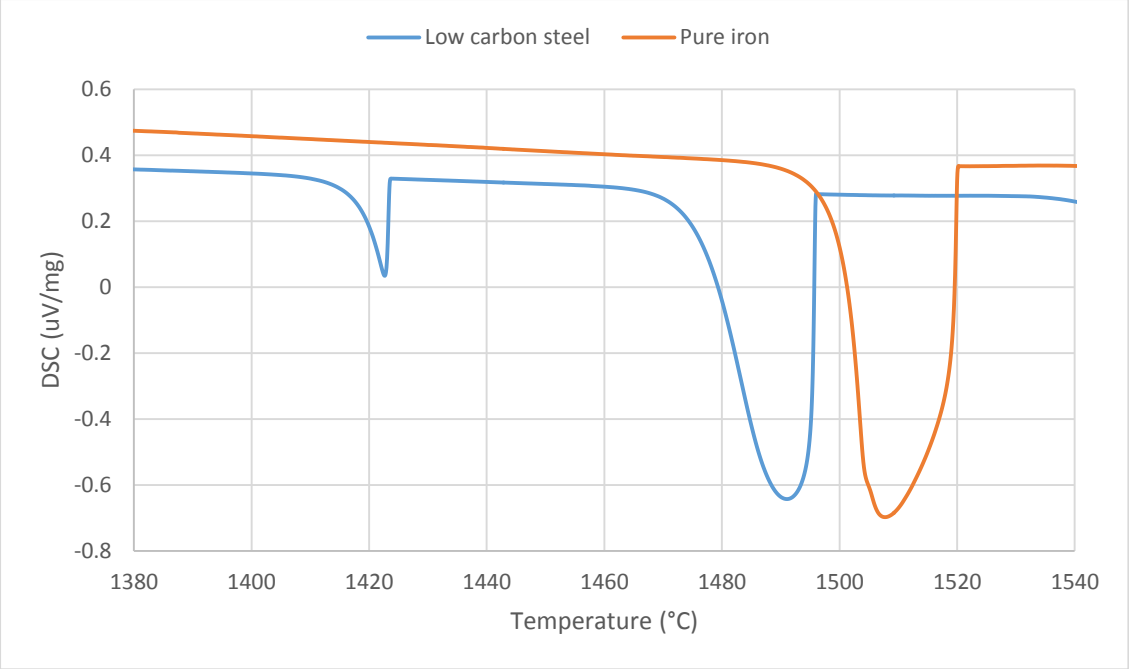


**Figure 2: DSC traces during cooling at 0.5 °C/s for the pure iron and low carbon steel used in this study.**

Figure 3a shows the measured radiated heat taken from a pixel from the surface of the molten sample during cooling at 1 °C/s of a pure iron sample. The temperature plotted is the recorded temperature measured by a type R thermocouple integrated in the crucible holder. It is observed that a linear decline in radiated heat can be seen initially. At 26s the heat emitted then starts to rise and is consistent with the start of solidification. In this case solidification will have started subsurface and therefore increasing the temperature of liquid at the surface of the droplet, this can be seen in Figure 3b-2 where the surface is still liquid (it should be noted that during the test an obvious change in the convention of the sample was observed in realtime). At 50s there is a sharp spike in radiated heat, this is likely to be attributed to the surface emissivity decrease from liquid steel to solid steel [16], with CSLM observation agreeing to this (Figure 3b-3). After this a continual decrease in the radiated heat is seen. Using the CSLM temperature measurement then solidification in this case

occurred between 1522 and 1495 °C. This is in good agreement with the DSC trace shown in Figure 2 which showed a solidification range of 1520 to 1495 °C. It should be noted however, unlike the DSC, enthalpy of fusion cannot be calculated from these curves as heat is not only lost from the surface, but also conducted through the crucible, and the proportion of this balance is not known.

As such a large change in the signal was seen at the latter stages of solidification (which is consistent with the surface solidifying) then the same analysis was used on a pixel in the crucible base, 0.5 mm away from the droplet (Figure 4). This curve shows a similar trace but without the final spike, this agrees well that the spike is attributed to a change in surface emissivity as the crucible will not undergo any significant changes in emissivity. The change in radiated heat here is therefore attributed to the conduction from the sample as the latent heat is given off during the droplets transformation. The significant temperatures are consistent between both sets of data.

In both Figure 3 and Figure 4 the red arrows depict the temperature at which solidification is predicted to start under equilibrium conditions [17]. It can be seen that in general there is good agreement allowing for a small degree of undercooling to occur.

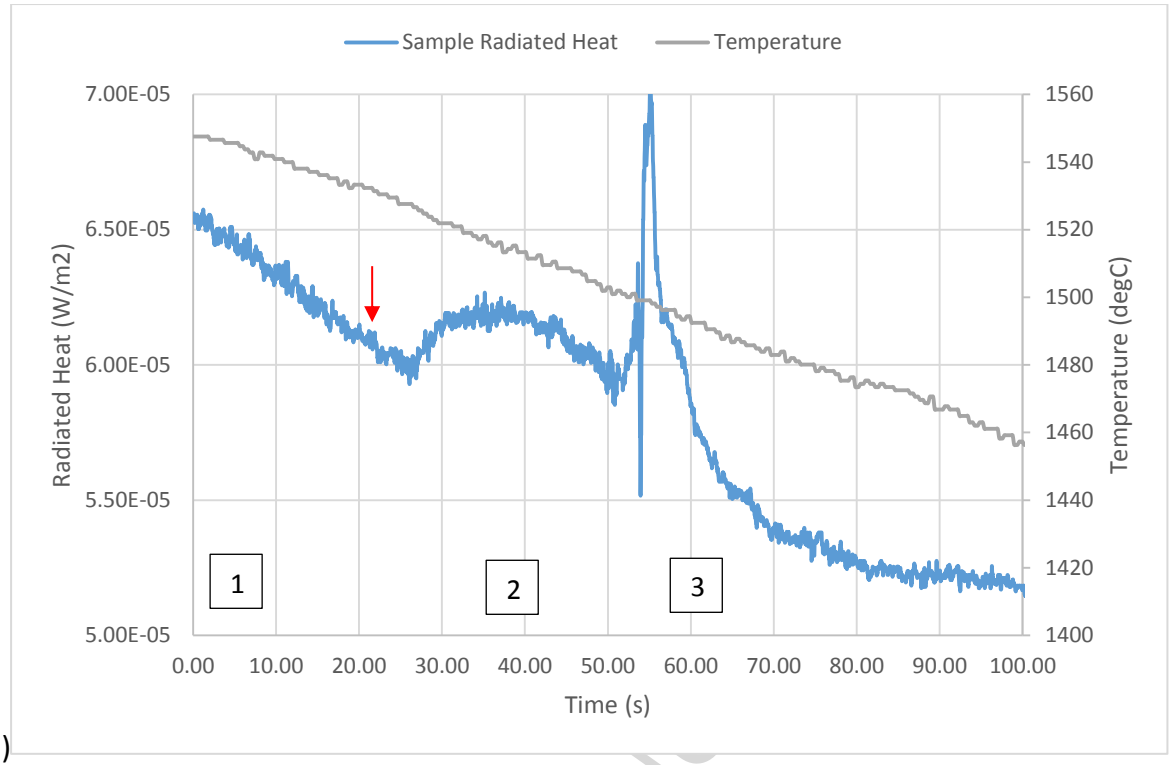


a)

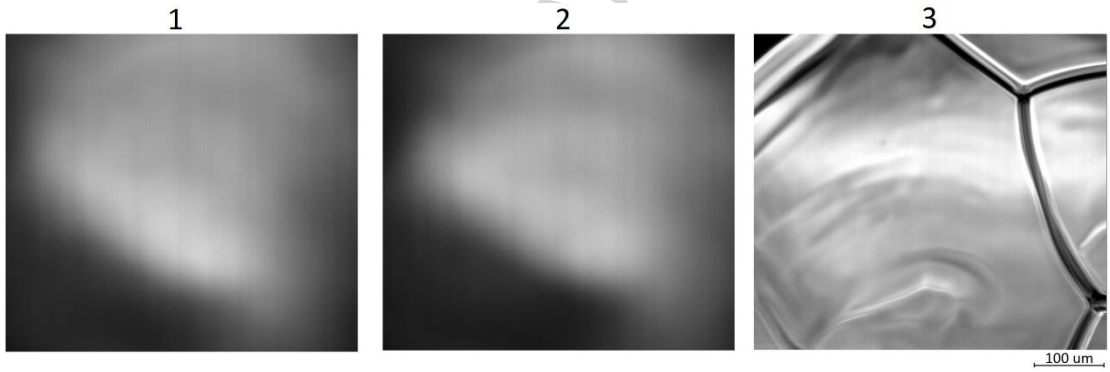


b)

**Figure 3: Showing a) the radiated heat measured by the thermographer during 1 C/s cooling of the pure iron sample. The red arrows depicts the equilibrium transformation start temperature. b) CSLM images corresponding to specific points in time during cooling shown in a).**

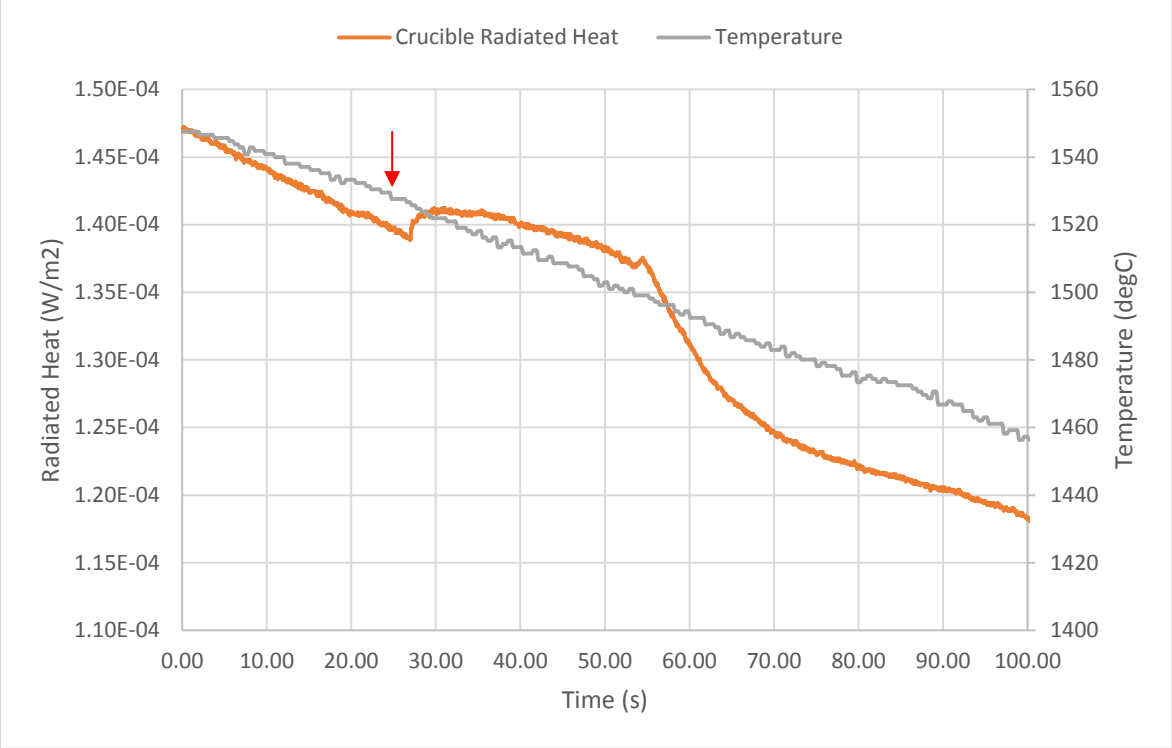


**Figure 4: Showing the radiated heat measured by the thermographer during 1 C/s cooling of the crucible base around 0.5 mm away from the sample. The red arrows depicts the equilibrium transformation start temperature.**

Figure 5a shows the radiated heat from the low carbon steel sample cooling at 1 C/s. Here it can be seen that the curves show a very similar trend to that of the pure iron however solidification can now be seen to start around 1473 °C and finishes around 1435 °C. A greater degree of undercooling was seen here however when compared to the DSC at 0.5 °C/s with solidification occurring from 1495 to 1472 °C.

The crucible curve (Figure 5) shows a very similar form to the pure iron, showing a small bump associated with the thermal conduction from the sample during transformation. However, the sample curve shows a reduced increase in temperature in the liquid prior to

the surface transforms. With alloys showing a “mushy zone” during transformation then this would be expected. One point of note is that the surface relies much more on quality of atmosphere, any inclusions/oxidation etc will cause variations in the emitted heat. The amount of emitted radiation is also a function of the position of the sample due to the curvature of the droplet, therefore the crucible base offers a more consistent point of reference.

At 168s in this sample is can be seen that another change in heat radiated which relates to a temperature of around 1390 °C. This is consistent with the transformation from delta ferrite to austenite (which can be observed in Figure 5b by the surface relief between images 3 and 4). The enthalpy change associated with the delta ferrite to austenite transformation is only 42 J/g compared to the 258 J/g change during solidification, and as such a much smaller peak is observed. Albeit small, these peak are seen consistently and agree well with observations from the CSLM laser imaging.

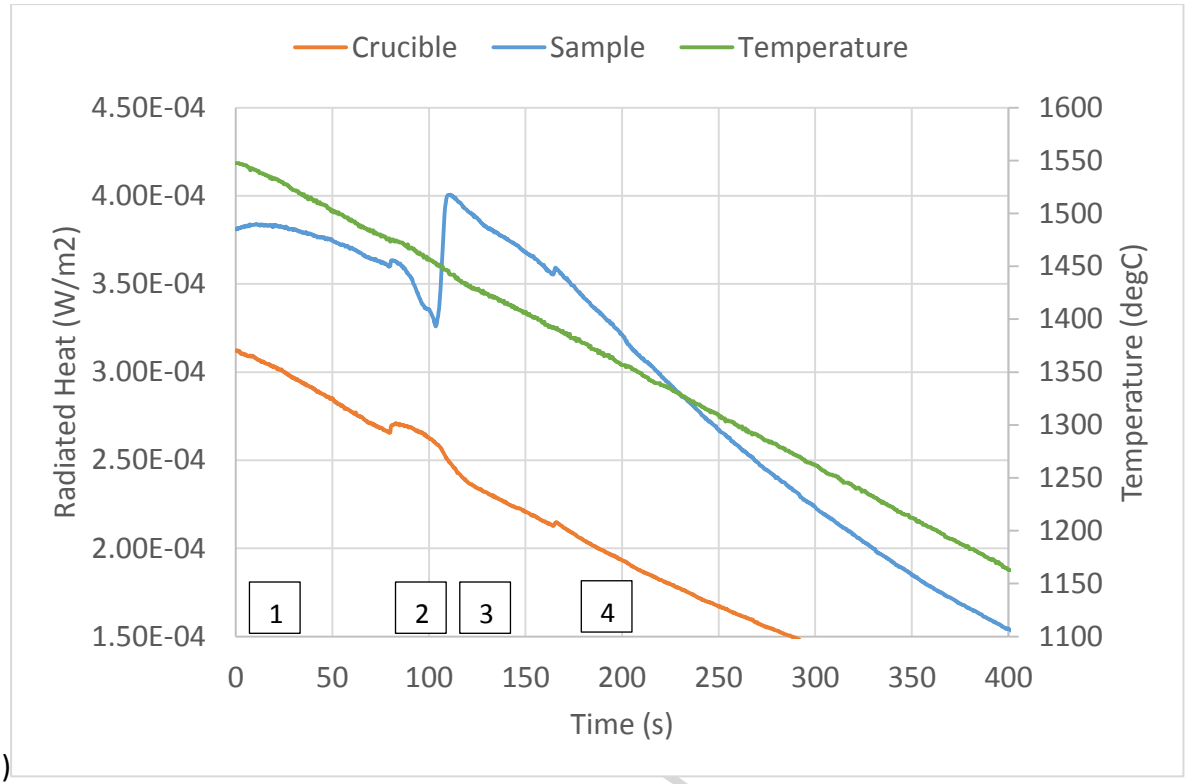


a)

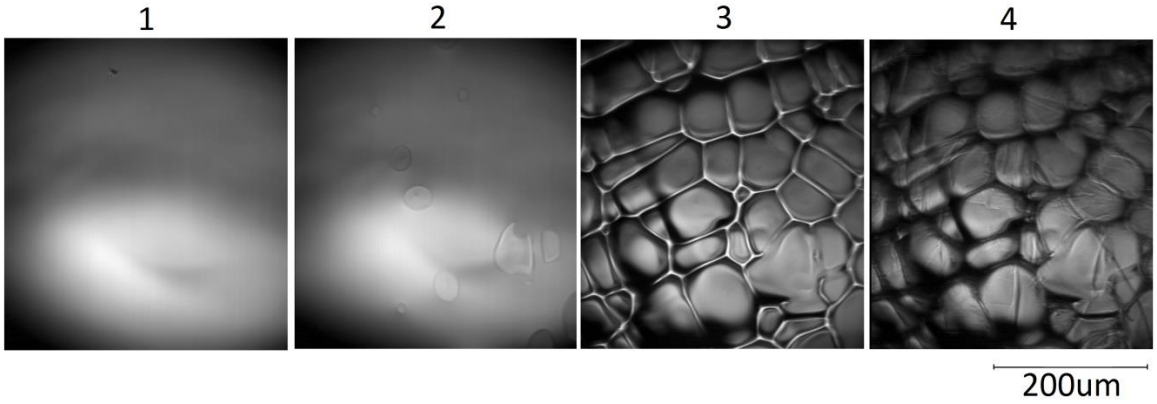


b)

**Figure 5: Showing a) Radiated heat emitted from the sample and crucible during a 1 C/s cooling of low carbon steel and b) CSLM time lapse images referring to times shown in a).**

Figure 6 shows the radiated heat traces for the 10 C/s cooling tests for both the pure iron and the low carbon steel. Clear distinction can be made from these traces can be made at

this higher cooling rate that is currently unobtainable through commercial calorimetry equipment (typically limited to around 0.25-0.5 °C/s at this temperature). Here a substantial amount of under cooling can be seen with the onset of solidification occurring at 1445 and 1434 °C for the pure iron and low carbon steel respectively (the red arrows in Figure 6 depict the predicted equilibrium onset of solidification). Coupled with the visual feedback from the laser of solidification, this offers a much better insight into the characteristics of solidification at these faster rates (e.g. solidification rate, degree of undercooling etc).

It is not being suggested that this technique replaces standard calorimetric techniques, but this addition to the CSLM allows for extra information to be obtained from the bulk rather that the highly localised surface seen through the laser microscope. This technique will be developed further in order to utilise the optical lenses of the microscope to gain detail into any thermal gradient that exist on a micro-scale (such as the temperature profile across a solidification interface).

The temperatures and rates stated in this paper are correct for the application of steels, however the CSLM cannot maintain these cooling rates all the way down to room temperature and therefore the same target cooling rates may not be achievable for aluminium without a helium quench (which is possible inside the CSLM however results in a fast, less controllable cool).

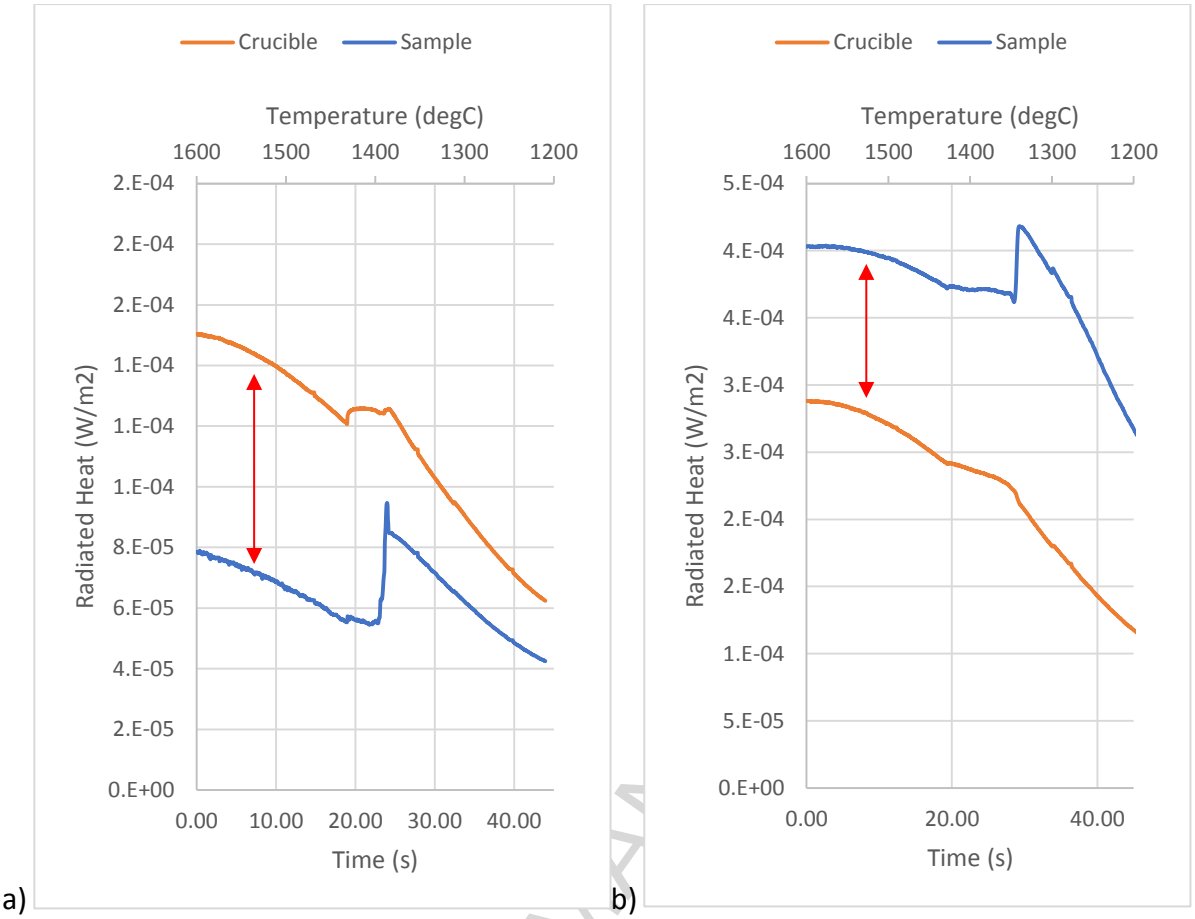


**Figure 6: Radiated heat of both the sample and crucible taken during 10 C/s cooling for a) pure iron and b) low carbon steel. The temperature from the CSLM has now been plotted on the secondary x-axis. The red arrow depicts the predicted equilibrium start to transformation.**

## 5. CONCLUSIONS

A technique has been detailed here that works as an addition to the standard confocal laser scanning microscope. The addition of infrared thermography has shown that it is possible to gain information about the latent heat of fusion seen during solidification and the heat of released during delta ferrite to austenite transformation of both pure iron and low carbon steel.

It has been seen that information about the bulk solidification can be obtained from the radiated heat from both the molten droplet and the crucible, which offer different but both useful information about the emitted heat. Furthermore, this technique is less constrained by heating and cooling rate of conventional calorimetry techniques (cooling rates up to 10 C/s have been used here).

An indication of the potential future uses for this technical has also been commented on in this paper.

## 6. ACKNOWLEDGEMENTS

The authors would like to thank EPSRC for funding (Grant number EP/M014002/1) and also WMG for their support and facilities.

## 7. REFERENCES

[1] Alcoa Micromill technology by Danieli, Http://www.danieli.com/en/products/products-Processes-and-Technologies/product-Lines/alcoa-Micromill-Technology-danieli_26_176.htm. (n.d.).

[2] S. Ge, M. Isac, R.I.L. Guthrie, Progress of Strip Casting Technology for Steel; Historical Developments, ISIJ Int. 52 (2012) 2109–2122. doi:10.2355/isijinternational.52.2109.

[3] M.I. and R.I.L.G. Sa GE, Progress in Strip Casting Technologies for Steel; Technical Developments, (n.d.). https://www.jstage.jst.go.jp/article/isijinternational/53/5/53_729/_article (accessed April 4, 2014).

[4] R.I.L. Guthrie, M.M. Isac, " THE NEAR NET SHAPE CASTING OF STEELS ; THE WAY FORWARD ?," (n.d.).

[5] N. Kikuchi, S. Nabeshima, T. Yamashita, Y. Kishimoto, S. Sridhar, T. Nagasaka, Micro-structure Refinement in Low Carbon High Manganese Steels through Ti-Deoxidation, Characterization and Effect of Secondary Deoxidation Particles, ISIJ Int. 51 (2011) 2019–2028. doi:10.2355/isijinternational.51.2019.

[6] H. Yin, H. Shibata, T. Emi, M. Suzuki, Characteristics of Agglomeration of Various Inclusion Particles on Molten Steel Surface, ISIJ Int. 37 (1997) 946–955. doi:10.2355/isijinternational.37.946.

[7] H. Yin, H. Shibata, T. Emi, M. Suzuki, "*In-situ*" Observation of Collision, Agglomeration

and Cluster Formation of Alumina Inclusion Particles on Steel Melts, ISIJ Int. 37 (1997) 936–945. doi:10.2355/isijinternational.37.936.

[8] N. Yuki, H. Shibata, T. Emi, Solubility of MnS in Fe-Ni Alloys as Determined by In-Situ Observation of Precipitation of MnS with a Confocal Scanning Laser Microscope, ISIJ Int. 38 (1998) 317–323. doi:10.2355/isijinternational.38.317.

[9] C. Slater, C. Davis, Using Confocal Scanning Laser Microscopy to Characterise As-Cast Microstructures Using Cooling Rates Representative of Thin Slab Direct Cast Steels ., LA Metall. Ital. February (2016).

[10] M. Reid, D. Phelan, R. Dippenaar, Concentric Solidification for High Temperature Laser Scanning Confocal Microscopy, ISIJ Int. 44 (2004) 565–572. doi:10.2355/isijinternational.44.565.

[11] P. Sridhar, S; Lee, P D; Rockett, Experimental techniques for in situ characterization of evolving solidification microstructures, AFS Trans. 110 (2002) 147–158.

[12] Y. Wang, S. Sridhar, M. Valdez, Formation of CaS on Al2O3-CaO inclusions during solidification of steels, Metall. Mater. Trans. B. 33 (2002) 625–632. doi:10.1007/s11663-002-0042-1.

[13] S. Griesser, M. Reid, R. Pierer, C. Bernhard, R. Dippenaar, In Situ Quantification of Micro-Segregation that Occurs During the Solidification of Steel, Steel Res. Int. 85 (2014) 1257–1265. doi:10.1002/srin.201300024.

[14] S. Griesser, C. Bernhard, R. Dippenaar, Effect of nucleation undercooling on the kinetics and mechanism of the peritectic phase transition in steel, Acta Mater. 81

(2014) 111–120. doi:10.1016/j.actamat.2014.08.020.

[15] D. Phelan, M. Reid, R. Dippenaar, Kinetics of the peritectic reaction in an Fe-C alloy, Mater. Sci. Eng. A. 477 (2008) 226–232. doi:10.1016/j.msea.2007.05.090.

[16] F. Cverna, Thermal Emittance, in: ASM Ready Ref. - Therm. Prop. Met., ASM International, 2002.

[17] Thermo-Calc Software TCFE7 Steels/Fe-alloys database version 7, (Accessed 08 Jan 2016), (n.d.).